







Characterization and quantification of adeno-associated virus capsid-loading states by multi-wavelength analytical ultracentrifugation with UltraScan

Amy Henrickson¹ , Xiaozhe Ding² , Austin G Seal³, Zhe Qu², Lauren Tomlinson⁴, John Forsey⁴ , Viviana Gradinaru² , Kazuhiro Oka^{3,5}  & Borries Demeler^{*,1,6} 

¹Department of Chemistry & Biochemistry, University of Lethbridge, Lethbridge, AB, T1K 3M4, Canada

²Division of Biology & Biological Engineering, California Institute of Technology, Pasadena, CA 91125, USA

³Gene Vector Core, Advanced Technology Cores, Baylor College of Medicine Houston, TX 77030, USA

⁴Pharmaron Biologics Ltd, Speke, Liverpool, L24 8RB, UK

⁵Department of Molecular & Cellular Biology, Baylor College of Medicine, TX 77030, USA

⁶Department of Chemistry & Biochemistry, University of Montana, Missoula, MT 59812, USA

*Author for correspondence: demeler@gmail.com

Aim: We present multi-wavelength (MW) analytical ultracentrifugation (AUC) methods offering superior accuracy for adeno-associated virus characterization and quantification. **Methods:** Experimental design guidelines are presented for MW sedimentation velocity and analytical buoyant density equilibrium AUC. **Results:** Our results were compared with dual-wavelength AUC, transmission electron microscopy and mass photometry. In contrast to dual-wavelength AUC, MW-AUC correctly quantifies adeno-associated virus capsid ratios and identifies contaminants. In contrast to transmission electron microscopy, partially filled capsids can also be detected and quantified. In contrast to mass photometry, first-principle results are obtained. **Conclusion:** Our study demonstrates the improved information provided by MW-AUC, highlighting the utility of several recently integrated UltraScan programs, and reinforces AUC as the gold-standard analysis for viral vectors.

First draft submitted: 30 May 2023; Accepted for publication: 4 September 2023; Published online: 25 October 2023

Keywords: adeno-associated virus • analytical buoyant density gradient equilibrium • gene therapy • multi-wavelength analytical ultracentrifugation • sedimentation velocity • UltraScan • viral capsid quantification • viral vector

Gene therapy is gaining increased attention for its potential to treat or cure a broad range of genetic diseases. Over the past few years, several gene therapy products have been approved by the EMA and the US FDA, while thousands more are candidates in clinical trials [1–3], demonstrating their importance in today's therapeutic arsenal. One of the most established vector systems used is the adeno-associated virus (AAV) [4] due to its minimal pathogenicity and broad clinical applicability [5], resulting in three FDA-approved AAV gene therapies to date [2]. The AAV capsid consists of about 60 viral protein subunits made up of VP1, VP2 and VP3, typically in a 1:1:10 ratio [6]. After the capsid is formed, the recombinant AAV genome containing the gene of interest is packaged as ssDNA into the capsids, resulting in full AAVs. Notably, this method relies on the efficient transfection of three or more unique plasmids into a single cell, resulting in the production of full capsids as well as unwanted by-products, including empty and partially filled capsids.

Product-related impurities such as empty capsids, a critical quality attribute, can induce antigen presentation in the cell, leading to increased immune responses and proteasomal degradation of viral capsids, potentially leading to therapeutic failure [7], while also competing with full capsids for cell receptor entry. Therefore, it is essential to accurately characterize AAV-loading states, and methodology must be developed to: efficiently purify full capsids from empty, aggregated and partially filled capsids; quantify gene therapy drug formulations for the precise amount

of full capsids compared with the other loading states; and identify contaminants. Previously developed analytical methods are limited in their ability to characterize or quantify product-related impurities [8]. Challenges encountered in the characterization of AAV formulations relate to the accuracy and resolution with which this quantification can be made, the throughput and cost of the analysis, and the sensitivity with which the measurement can be made [9]. Other AAV characterization techniques that focus on the characterization of the capsid-loading states include transmission electron microscopy (TEM), size-exclusion and anion exchange chromatography and mass photometry (MP) [10]. PCR and ELISA are used for the quantification of capsid titers [11]. Each method provides satisfactory results, but with various limitations [10,12,13]. The ability of analytical ultracentrifugation (AUC) to characterize and accurately quantify the composition of an AAV sample, in a single experiment with minimal sample preparation, is a significant advantage of AUC [14]. AUC can detect empty, partially filled and filled capsids, and contaminants such as free nucleic acids, DNA length heterogeneity in partially filled capsids, aggregates and full capsids with nucleotide loads fractionally greater than one genome [15]. In addition, the UltraScan software is designed to adhere to Title 21 of the Code of Federal Regulations Part 11 (21 CFR Part 11) requirements, allowing AUC to be integrated into a current GMP environment [16].

Current AUC methods primarily employ sedimentation velocity (SV) experiments for AAV characterization [14,17,18]. SV measures the transport of macromolecules dissolved in solution; derives the sedimentation and diffusion coefficients of all species in a mixture; and reports their partial concentrations, buoyant molar masses and shape factors. Despite the popularity of AUC in characterizing empty/full capsid ratios, several shortcomings exist. First, the most often cited SV design only measures between one and three wavelengths (generally 230, 260 and 280 nm) and at times is matched with Rayleigh interference experiments [17]. These methods overestimate filled capsids due to protein and nucleic acid spectral overlap [19]. Therefore quantification is always distorted when the DNA and protein extinction coefficients are not separated [20], which is only possible when measuring in multi-wavelength (MW) mode [21]. Secondly, SV is a low-throughput technique, and analysis is considered difficult, requiring significant training and time investment. Thirdly, SV experiments require relatively large amounts of sample (~0.5 ml/experiment, 0.3–0.9 optical density [OD] at 260–280 nm). In an effort to reduce sample requirements, analytical band centrifugation has recently been explored as an alternative to characterize AAV composition [22,23].

In this study, we report improvements to AUC methods used for the characterization and quantification of AAVs. Specifically, we applied MW analysis to SV and analytical buoyant density equilibrium (ABDE; sometimes also called density gradient equilibrium) experiments with AAVs. With the availability of new and improved AUC instruments, MW analysis has been demonstrated to be a powerful new tool for the characterization of the interactions between two or more molecules with distinct absorbance profiles [19,24–28]. AAV consists of a protein coat and encapsulated DNA, two molecules with unique but overlapping chromophores. Hence MW-AUC is ideally suited to characterize and quantify the composition of AAV samples. MW-AUC methods take advantage of the optical system in the latest Beckman Optima™ analytical ultracentrifuge and new software modules developed for UltraScan [29]. The value of SV analysis performed at multiple wavelengths, and manually analyzed, in a labor-intensive approach was previously demonstrated for the analysis of AAVs by Maruno *et al.* [22,24]. Richter *et al.* also demonstrated the ability of MW-AUC to obtain DNA insert length and derived wavelength-specific correction factors for the respective insert size, and compared their results with those from several characterization methods [18]. Recently developed UltraScan software modules now largely automate the MW-AUC analysis workflow, reducing the requirement for training and time spent analyzing AUC data [16,21,30–32].

MW-AUC offers a second spectral dimension for the separation of macromolecules in solution, in addition to the traditional hydrodynamic separation, which can resolve and identify loading states, distinguish full capsids from contaminants and resolve unique species with high precision. SV experiments provide separation based on mass, size, anisotropy and density. SV offers access to a large particle size range and excels by detecting even small amounts of contaminants. ABDE experiments separate AAV-loading states in a CsCl gradient based only on their density. ABDE experiments offer high resolution, sensitivity and throughput, with minimal sample requirements and rapid data analysis [31,33,34]. Below, we apply MW capabilities to SV and ABDE experiments for the analysis of AAV capsid-loading states and compare our results with TEM and MP measurements. We show that both MW-AUC methods achieve excellent agreement with TEM and MP, although AUC offers improved statistics due to bulk observation and enhanced resolution while reducing sample requirements.

Materials & methods

AAV production

AAV8 were prepared by the Gene Vector Core at Baylor College of Medicine (TX, USA) using a published method [35]. HEK293T cells were maintained in DMEM (cat. no. CM002-050, GenDEPOT, TX, USA) supplemented with 10% fetal bovine serum (Avantor Seradigm, PA, USA) and antibiotic–antimycotic (cat. no. CA002-100, GenDEPOT), in 15-cm dishes at 37°C, 5% CO₂ in a humidified CO₂ incubator. AAV was packaged by a three-plasmid transient transfection with iFectin Poly DNA Transfection Reagent (cat. no. I7200, GenDEPOT). A total of 8 µg of DNA was combined with iFectin, and 1 ml of the DNA cocktail was overlaid per dish. Cell-associated and media-secreted AAV were collected separately 72 h after transfection. Cell-associated AAV was recovered by cell lysis using 5% deoxycholate and subsequently treated with DNase I and RNase. Media-secreted AAV was precipitated with 40% PEG8000 supplemented with 2.5 M NaCl to a final concentration of 8% PEG. Both AAV fractions were combined and purified by CsCl ultracentrifugation as described by Ayuso *et al.* [36].

AAV9:CAG-GFP was generated at the CLOVER Center, Caltech (CA, USA), by triple transfection of HEK293T/17 cells (American Type Culture Collection, VA, USA; cat. no. CRL-11268) cultured in 15-cm dishes [37,38] and purified using a precipitation-based method. Briefly, 3 days after transfection, the producer cells were lifted by adding 10 mM EDTA to the media. After being spun down at 2000 × g for 10 min, viral particles in the cell pellets were purified with the AAVPro purification kit (TaKaRa Bio, CA, USA, cat. no. 6675) according to the manufacturer's instructions. AAV9:CAG-mNeonGreen samples were produced in HEK293T/17 cells cultured in 15-cm dishes with the triple transient transfection method and then purified by iodixanol gradient ultracentrifugation as previously described [37]. Virus titers were measured using qPCR targeting the WPRE region of the viral genomes [37].

Empty AAV5 was generated by Pharmaron (Liverpool, UK) using the HEK293 cell line and triple transfection. Following harvest, the feedstock was clarified and subsequently purified. The purification process consists of three chromatography steps: affinity chromatography, cation exchange chromatography and anion exchange chromatography.

Electron microscopy

TEM analysis for AAV8 BCM #1 was performed by the Baylor College of Medicine CryoEM Core. Samples were stained on Quantifoil 2/2 200Cu⁺ 8-nm ThinC grids (Quantifoil Micro Tools GmbH, Jena, Germany) using a 2% uranyl acetate solution (Sigma Aldrich, MO, USA). The images were taken using a 200-kV JEOL 2200FS electron microscope (JEOL Ltd, Tokyo, Japan) using a Direct Electron DE-20 camera (Direct Electron, CA, USA). The images were then analyzed by FIJI ImageJ software (NIH, MD, USA).

AAV9:CAG-mNeonGreen 1 TEM experiments were performed in the Caltech CryoEM center. Samples were stained on Carbon Type-B 200 Cu grids (Ted Pella, CA, USA) using 3% uranyl acetate solution (Sigma Aldrich). The images were taken by a Tecnai T12 120 kV electron microscope (FEI, OR, USA) using a Gatan 2k × 2k CCD (Gatan, CA, USA).

Mass photometry

An AAV5 empty sample was acquired in triplicate on a Refeyn Samux mass photometer (Oxford, UK). A microscope coverslip was cleaned consecutively in Milli-Q[®] water, isopropanol and Milli-Q water prior to mounting a silicone gasket on the coverslip; then 10 µl of phosphate-buffered saline (PBS) was added to a gasket well and the instrument was focused and locked. Next, 10 µl of AAV5 empty reference sample was added to the PBS solution for a final AAV concentration of 2×10^{11} particles/ml. The sample in the well was aspirated using a pipette prior to acquisition of data. Analysis of the data was performed in DiscoverMP (Oxford, UK), where an AAV mass calibration was applied to convert the measured ratiometric contrast (between scattered and reflected light) to mass. Because the masses for both empty and full particles are known, the empty:full ratios can be determined by this method.

Analytical ultracentrifugation with MW SV detection

MW-AUC SV experiments were performed in a Beckman Coulter Optima analytical ultracentrifuge (Beckman Coulter, IN, USA) at the Canadian Center for Hydrodynamics at the University of Lethbridge. Samples were diluted to 0.3–0.4 OD at 260 nm with dPBS (Fisher Scientific, 14190144, WL, USA). Standard Beckman 1.2-cm epon-charcoal centerpieces, fitted with quartz windows, were filled with 460 µl of sample. In each experiment, a single cell was measured, and loaded with two samples, utilizing both the sample and reference channel, and

measured in intensity mode. AUC cells were loaded into an AN60Ti rotor and equilibrated at 4°C for 1 h before the rotor speed was increased to 14.5 kr.p.m. and scan collection began. A speed between 14.0 and 14.5 kr.p.m. will maximize the number of scans collected, because the flash lamp rate and rotor speed are synchronized at this speed, reducing the scanning time to ~8 s per channel of each cell. A temperature of 4°C was used to minimize the density variation in response to small, local temperature changes, which nearly eliminates sample convection during the run. Convection can occur in experiments where large analytes are measured at low rotor speeds in dilute buffers when the Optima AUC's temperature control is activated [39]. The reduced temperature also increases the buffer density and viscosity, resulting in slower sedimentation and permitting additional data to be collected in MW mode. Intensity data were collected from both channels of a single cell, from 240 to 290 nm, every second wavelength. All data were analyzed using UltraScan 4.0 [29] as described previously [21,40]. Briefly, each triple (data from a single cell, channel and wavelength) was analyzed using two-dimensional spectrum analysis (2DSA) [41,42], which removes the time and radially invariant noise in the intensity data, fits the boundary conditions (meniscus and bottom of the cell) and refines the final model using an iterative approach. Residuals from the iteratively refined 2DSA models were examined for randomness and used to generate a time-synchronized sedimentation profile for each wavelength, which was used for MW deconvolutions [20,21,32].

Diffusion-corrected sedimentation coefficient profiles were generated using the enhanced van Holde–Weischet analysis [43] implemented in UltraScan [29] from the deconvoluted SV data. Dual-wavelength AUC results were obtained from the same MW-SV experiments, but using only the iterative 2DSA results from the 260- and 280-nm triples. The buffer density and viscosity corrections were calculated with UltraScan using the partial concentration of each buffer component.

Analytical buoyant density equilibrium

ABDE with AAV samples was performed in CsCl density gradients. ABDE experiments provide high resolution information on AAV-loading states, while requiring a significantly reduced amount of AAV sample compared with SV experiments. Like SV experiments, ABDE experiments can also be performed in MW mode to add spectral information to separate and quantify protein and DNA signals. ABDE experiments distinguish solutes based on their buoyant densities in a density gradient and produce sharp peaks for each solute that are easily quantifiable with the ABDE peak fitter in UltraScan, which calculates the density of each peak based on peak position by calculating the density gradient profile [31]. The peaks will occur at the positions where the solutes' densities equal the density of the gradient. Together, MW and density characterization provide an unambiguous, orthogonal AAV capsid characterization method.

ABDE experiments were performed in a Beckman Coulter Optima analytical ultracentrifuge at the University of Lethbridge. Samples were diluted between 0.2 and 0.25 OD at 260 nm (measured in a 1-cm path length), with a final CsCl density of 1.36 g/ml, unless mentioned otherwise, prepared in 10 mM Tris (pH 8.0) buffer and measured at 60 kr.p.m. Titanium 3-mm centerpieces (Nanolytics Instruments, Potsdam, Germany) were assembled in standard Beckman Coulter cell housings, fitted with sapphire windows and one 3-mm spacer above and below the centerpiece to align the centerpiece fill holes with the fill holes of the cell housing. For accurate quantification, the OD needs to remain within the dynamic range of the detector (0.1–0.9 OD for most wavelengths). The 3-mm centerpieces serve two purposes. First, by reducing the path length from the typical 12-mm cell used in SV experiments to 3 mm, only one-quarter of sample volume is required. Second, a reduced path length significantly decreases the radial refraction error generated by the lens-shaped CsCl gradient, which has a high refractive index.

The density difference generated in the gradient between the meniscus and the bottom of the cell depends on the centrifugal force (F), which is given by $F = m\omega^2r$, where m is the mass of the sedimenting particle, ω is the angular velocity and r is radius. Therefore, faster rotor speeds and longer columns provide the maximum density range and solute separation. In this configuration, eight samples can be measured simultaneously by utilizing both channels of the cells and all four rotor holes. When measuring with the AN50Ti rotor, 16 samples can be measured in a single run, but only up to 50 kr.p.m. It should be noted that as the rotor speed is decreased, the gradient becomes shallower, increasing the CsCl concentration near the meniscus compared with high-speed runs. Therefore when rotor speeds are decreased, the concentration of CsCl required to visualize empty capsids may also need to be decreased, otherwise the empty AAVs peak will not separate from the meniscus.

For ABDE experiments, scans were collected in intensity mode at equilibrium, from 236 to 288 nm every second wavelength for a total of 27 wavelengths. However, because the sample at equilibrium no longer changes its distribution in the gradient, unlimited time exists to collect up to 100 wavelengths per channel, which is possible

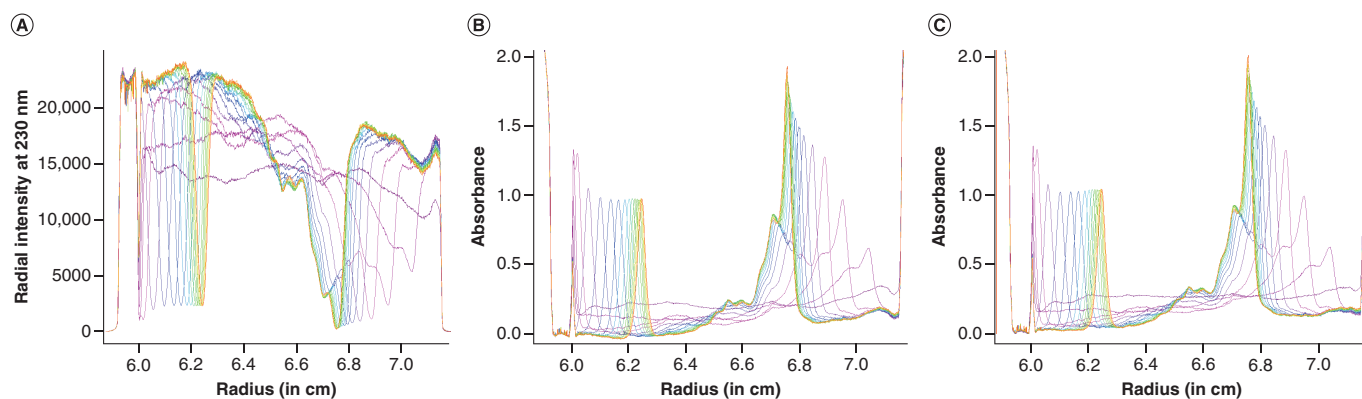


Figure 1. Noise correction of an analytical buoyant density equilibrium adeno-associated virus experiment. (A) Raw analytical buoyant density equilibrium intensity data from an adeno-associated virus sample approaching equilibrium, collected on the Optima™ AUC (only a single wavelength is shown). **(B)** Pseudo-absorbance conversion of data shown in **(A)** without time-invariant noise correction. **(C)** The same data after processing with the UltraScan's noise-correction module (Pseudo-Absorbance). The color gradient indicates time.

with UltraScan's data acquisition software for the Optima AUC. Data collection was performed throughout the experiment to determine when equilibrium was reached, but only the last scan from each wavelength, after the CsCl gradient was established, was used in the analysis. The gradient was deemed established after the solute peaks stopped shifting, approximately after 5 h at 60 kr.p.m. and at 20°C. Viral particles are relatively large compared with typical proteins, resulting in smaller diffusion coefficients and narrower peaks in an ABDE experiment. The width of the peaks formed in an ABDE experiment is directly proportional to the diffusion coefficient of the analyte and the temperature, and inversely proportional to the viscosity of the solvent. Given that AAV capsids have approximately the same size and shape regardless of their cargo load, and the temperature is constant, the width of each capsid peak is only a function of the local viscosity and density at a particular gradient position, which is primarily a function of the local CsCl concentration. Narrow peaks improve baseline resolution between peaks and reduce the amount of sample needed up to 40-fold compared with SV experiments.

For ABDE experiments, all data of interest are time-invariant. Hence, time-invariant/radially-invariant noise corrections as performed in SV experiments [44] cannot be used. Therefore a new noise-processing module was developed in UltraScan, called Pseudo-Absorbance, to process the time- and radially-invariant noise contributions [30]. The Pseudo-Absorbance module in UltraScan offers extensive baseline processing features that allow experimental data to be collected in intensity mode, removing time- and radially-invariant noise, and avoiding the amplification of stochastic noise by a factor of $\sqrt{2}$ [30,40]. The module converts intensity data to pseudo-absorbance data using the time-invariant intensity fingerprint of the photomultiplier tube in the Optima AUC as a function of radius and wavelength. This process extracts the time-invariant background signal from experimental data for each wavelength without the addition of stochastic noise, avoiding the use of a buffer channel for absorbance subtraction. As a result, the signal-to-noise ratio and precision of ABDE data are significantly enhanced. At the same time, the capacity of the instrument is doubled, because the reference channel can be used for another sample [30,40]. The effect of the noise-processing algorithm is illustrated in Figures 1 & 2. Figure 1A shows the samples approaching equilibrium measured in intensity. Figure 1B shows the data after conversion to pseudo-absorbance, but without any noise correction, while Figure 1C shows the data after noise correction, which corrects the baseline of the experiment to zero absorbance. In Figure 2, the effect of time-invariant noise contributions resulting from the photomultiplier tube can be seen clearly in the negative baseline observed near 6.2 cm in the red line. Noise processing in UltraScan restores an accurate baseline and recovers reliable peak amplitudes across the entire radial domain. After pseudo-absorbance conversion, the ABDE experiments are edited by selecting the meniscus and cell bottom positions and are spectrally deconvoluted into the spectral contributors, protein and DNA, as explained below.

The ABDE experiments can be analyzed with a recently added module in UltraScan for peak fitting [31]. This program calculates the integral and buoyant density of each analyte from its peak size and position, and other experimental parameters such as the meniscus position, bottom of the cell, gradient-forming material properties and concentration and the rotor speed. Because the density of each analyte is constant, even when any of these experimental parameters are varied, this calculation provides an unambiguous and reproducible

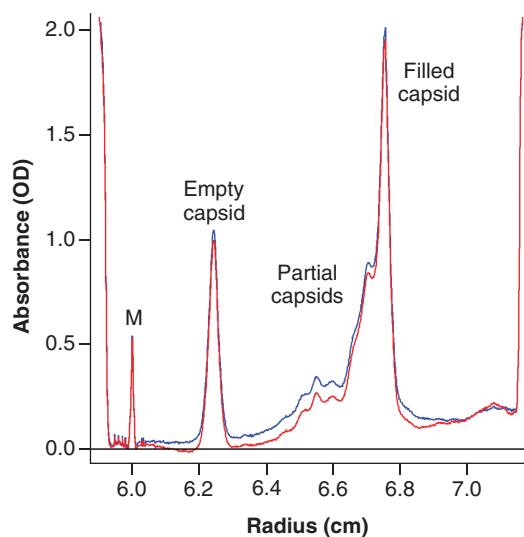


Figure 2. Effect of time-invariant noise correction. Shown is the last scan of the analytical buoyant density equilibrium experiment shown in Figure 1. Red: without time-invariant noise correction. Blue: with time invariant noise correction. Note the negative absorbance for the uncorrected scan near 6.2 cm. M: Meniscus position; OD: Optical density.

characterization of each analyte. Together with the MW characterization, this approach provides a very high precision for AAV characterization. For accurate quantification of capsid peaks, it is essential to also process ABDE baseline contributions from CsCl refractive artifacts and potential absorbing contaminants in the sample or buffer, as described by Savelyev *et al.* [30], before processing the data with the peak integration module of UltraScan [31].

MW deconvolution

MW-AUC data were deconvoluted into the spectral contributions from each absorbing analyte (protein and DNA) as described previously [20,21]. If the buffer or gradient-forming material absorbs in the measured wavelength region, it must be included in the spectral deconvolution. The amounts of sample required to measure pure AAV protein and DNA extinction spectra are difficult to obtain. Instead, we chose to measure a dilution series from albumin (Bio Basic cat. no. D0024, Markham, Canada), serving as a pure protein standard, and a highly purified DNA plasmid between 240 and 290 nm. A GENESYS™ 10S benchtop spectrophotometer (Thermo Fisher Scientific, WI, USA) was used to collect all extinction profiles. When measuring between 240 and 300 nm, the absorbance spectrum from albumin is sufficiently similar to that of the viral capsids because only tryptophan and tyrosine contribute to the spectrum in this range; hence it can be used instead of the empty capsid spectrum to obtain a pure spectrum. However, when measuring below 240 nm, the capsid absorbance also depends on the peptide backbone absorption, whose molar absorptivity is primarily a function of the number of peptide bonds in the protein. Because the ratio of the number of peptide bonds and the number of aromatic side chains is not constant, measurements that include wavelengths below 240 nm require a purified empty capsid protein spectrum. A sum of Gaussian terms was fit to each dilution series and scaled to 1.0 OD at 280 nm for protein and 260 nm for nucleic acid, using the Spectrum Fitter program in UltraScan [29]. Whenever MW-AUC data are deconvoluted into contributions from individual chromophores, the 3D-residuals viewer from UltraScan should be used to assess the quality of the decomposition to make sure the basis functions are properly representing the original spectrum [32]. An example of our MW deconvolution fits for a single scan can be seen in [Supplementary Figure 1](#), and for a single radial position in [Supplementary Figure 2](#). It is recommended that the user view each scan and radial position to ensure random fits and low root mean square deviations.

Because accurate molar extinction coefficients are also difficult to obtain for single-stranded DNA cargo, packaged inside a protein capsid, we have adopted a different approach for ABDE experiments: we chose to normalize the protein and DNA extinction vectors used for spectral deconvolution such that spectral contributions from protein and DNA observed for the filled capsid species are equal in magnitude. Filled capsids have a known density and are typically the major species in AAV preparations, and hence provide sufficient signal and are readily identified. Comparison of the normalized absorbance facilitates identification of empty capsids (no spectral contribution from DNA), partially filled capsids (spectral contribution from protein exceeds the DNA contribution) and filled capsids (protein and DNA spectral contributions are equal in amplitude), as well as overloaded species (spectral contribution from DNA exceeds the protein spectral contribution). Precise molar extinction coefficients are generally not available

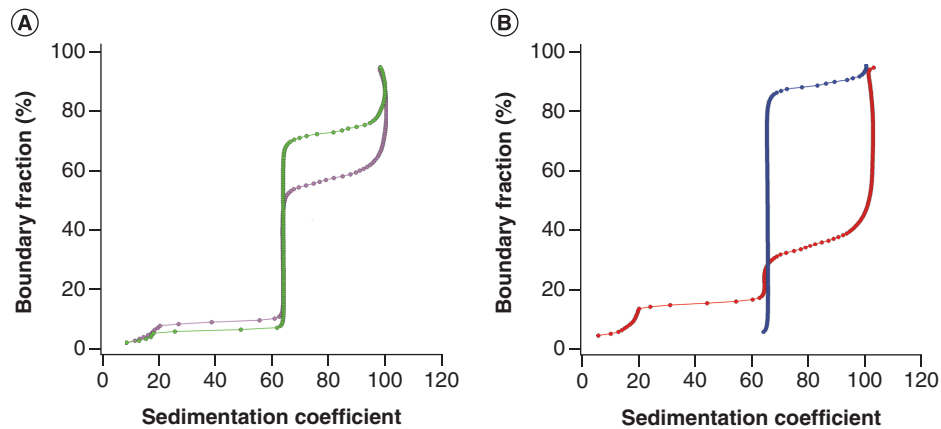


Figure 3. Comparison of the enhanced van Holde–Weischet distributions of the 260/280 nm and multi-wavelength analytical ultracentrifugation results. SV AUC data for AAV9:CAG-GFP analyzed using (A) only the 260 (pink) and 280 nm (green) wavelengths and (B) the deconvoluted MW SV AUC method (blue: 280 nm; red: 260 nm). AAV: Adeno-associated virus; AUC: Analytical ultracentrifugation; MW: Multi-wavelength; SV: Sedimentation velocity.

and are not needed to perform the identification of loading states of AAV peaks. Using this approach, it is possible to uniquely determine the relative amounts of protein and DNA of each capsid species present in a mixture by comparison with a filled capsid.

Results

SV experiments

To determine the composition of AAV formulations, we performed MW-AUC SV experiments, which resolve AAV capsids and contaminants based on their sedimentation coefficient profile and spectral properties, offering excellent resolution. MW-AUC (collected every second wavelength from 240 to 290 nm) separates the results into the spectral contributors of AAV, the protein capsid and DNA transgene, generating individual hydrodynamic distributions for each macromolecule [21]. The empty:full capsid ratio can be directly quantified from the integral sedimentation coefficient distributions generated in the van Holde–Weischet analysis for the MW data [43]. Figure 3 compares the 260- and 280-nm van Holde–Weischet distributions for an AAV9:CAG-GFP sample with the MW-AUC SV results. Figure 3A suggests that 45% of the total concentration sediments as a 100 S species (filled capsids) and 45% as a 65 S species (empty capsids) when measured at 260 nm, while the 280-nm results suggest that 30% of the total concentration sediments as a filled capsid and 65% as an empty capsid. The remainder (10% for the 260-nm measurement and 5% for the 280-nm measurement) sediments at a lower sedimentation coefficient (<20 S), and its identity is unknown. The MW-AUC analysis is shown in Figure 3B. Here, the protein and DNA signals are separated into individual van Holde–Weischet distributions, which reflect the relative contribution of each macromolecule in the hydrodynamically separated data. For filled capsids, both DNA and protein signals contribute, while empty capsids only show protein contribution and partially filled capsids show both protein and DNA signals, with an excess of protein signal. Free nucleic acids are identified by the absence of co-migrating protein signal. Based on the protein signal, the MW-AUC results show that the relative concentration of the 100 S species (filled capsids) contributes only 10% of the total protein signal, while the remaining 90% of the protein signal sediments at 65 S (presumably empty capsids). The DNA signal shows that 65% of the DNA co-migrates with the 100 S species (filled capsids) and 20% co-migrates with the 65 S species, indicating that the 65 S species is not truly an empty capsid but contains a small amount of bound nucleic acid, allowing us to classify the 65 S species as a partially filled capsid. The remaining 15% of the DNA signal sediments slower than 20 S, but without any co-migrating protein contribution, identifying the slower species as free nucleic acid. These MW-AUC results demonstrate several key points. First, because absorbance spectra for protein and DNA have significant overlaps in the range 200–300 nm, single-wavelength analysis will always add the DNA signal to the signal of the protein species and overestimate the amount of full capsids. Second, the presence of a small amount of DNA signal in the 65 S species demonstrates that the S-value alone is insufficient to classify capsids as empty, partially filled or filled capsids, and that quantification of AAV capsid-loading states using single-wavelength AUC is inherently unreliable.

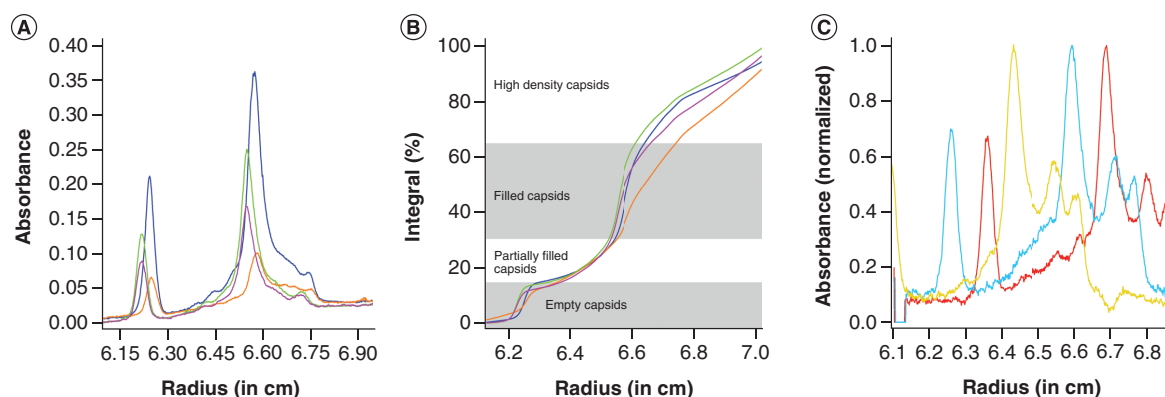


Figure 4. Analytical buoyant density equilibrium optimization. Only the deconvoluted protein absorption pattern is shown for ABDE experiments for ease of reading. **(A)** Deconvoluted protein signal from ABDE experiments of AAV9:CAG-mNeonGreen 1 at four different AAV concentrations (3.64×10^{12} [orange], 6.36×10^{12} [green], 9.55×10^{12} [pink] and 1.36×10^{13} vg/ml [blue]). **(B)** Normalized integral distribution of the data shown in **(A)**, demonstrating that the relative concentrations of each species remain constant. **(C)** Normalized results for AAV9:CAG-mNeonGreen 2 in different CsCl concentrations (1.35 [red], 1.36 [cyan] and 1.38 g/ml [yellow]). ABDE: Analytical buoyant density equilibrium; AAV: Adeno-associated virus.

Third, MW-AUC analysis is required to accurately identify any contaminants as proteins, DNA, or protein–DNA complexes. Fourth, in cases where molar extinction coefficients are available, the protein and DNA distributions will be reported in molar units and MW-AUC can report directly the number and ratio of protein and DNA molecules in each capsid species. Because protein and DNA spectra have significant spectral overlap, failure to account for the relative contribution of both biopolymers will always lead to an overestimation of the filled capsids, regardless of wavelength used. Examples of the normalized spectra for AAV5 and DNA are shown in [Supplementary Figure 3](#). The relative error for overestimating the amount of filled capsids varies as a function of wavelength. For the case shown in [Supplementary Figure 3](#), the relative error at 280 nm is 0.91:1, 2.89:1 at 260 nm and 0.124:1 at 230 nm. While the quantification error is reduced at 230 nm, it is not zero, and single-wavelength measurements will always yield incorrect relative quantities when the extinction contributions from DNA are not properly taken into account. MW-AUC is the only reliable approach to mitigate this problem.

Analytical buoyant density equilibrium

ABDE experiments use a density gradient-forming material to separate analytes based on their densities, supporting reduced sample volume requirements and increased throughput. The linearity of the ABDE method was evaluated to test its ability to obtain proportional results for different AAV concentrations ([Figure 4A & B](#)). For clarity, only the deconvoluted protein signals are shown in [Figure 4](#). AAV9:CAG-mNeonGreen 1 was measured at four concentrations ranging between 3.64×10^{12} and 1.36×10^{13} vg/ml (0.11–0.40 OD at 260 nm in a 1-cm path length). The deconvoluted protein signals from each concentration are shown in [Figure 4A](#) (without normalization), and their normalized integral distributions are shown in [Figure 4B](#), which confirm equal ratios of empty, partially filled and filled capsids. A minor shift in radial position across all peaks is seen in [Figure 4A](#), which results from a slight variation in loading volume. For all concentrations, empty capsid peaks appear at a density between 1.19 and 1.20 g/cm³ (6.17–6.3 cm) and contribute approximately 15% to the total signal, while the partially filled capsids contribute approximately 15% of the signal and appear between 6.35 and 6.5 cm. The filled capsids appear between 6.5 and 6.65 cm and have peak densities between 1.30 and 1.31 g/cm³ and contributed approximately 35% of the total signal. Unexpectedly, two discrete higher-density species are identified between 6.65 and 6.8 cm with peak densities between 1.37 and 1.38 g/cm³ that contribute approximately 35% of the signal; these were identified in all samples that contained filled AAVs and are further discussed below.

To optimize the run time and AAV peak formation, various CsCl concentrations, rotor speeds and CsCl column lengths were tested. The effect of varying CsCl concentrations on peak distributions for sample AAV9:CAG-mNeonGreen 2 is seen in [Figure 4C](#). As the CsCl concentration is increased from 1.35 g/ml (red) to 1.36 g/ml (cyan) to 1.38 g/ml (yellow), all AAV peaks shift to the left. At a CsCl concentration of 1.36 g/ml, an optimal distribution of AAV peaks was observed (at 60 kr.p.m.) because it positions empty, partially filled and filled capsids

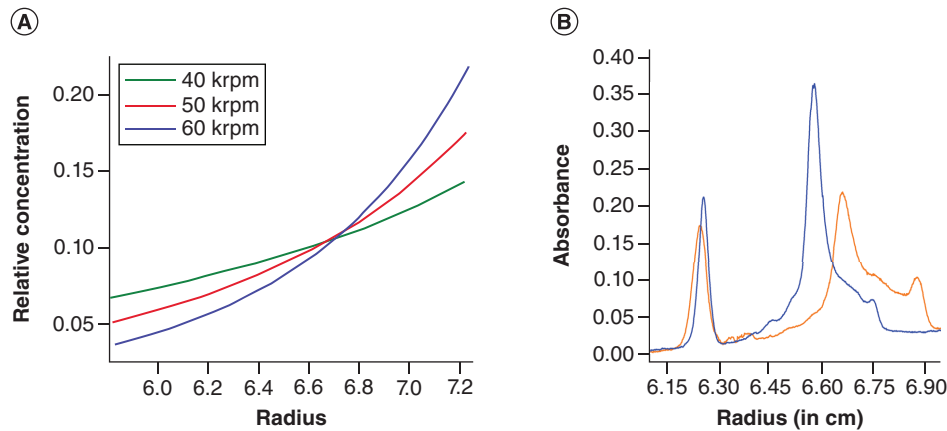


Figure 5. The effect of speed on CsCl gradient formation. (A) Simulated gradient shapes for CsCl at 40,000 (green), 50,000 (red) and 60,000 r.p.m. (blue). (B) AAV9:CAG-mNeonGreen1 measured at 60,000 (blue) and 50,000 r.p.m. (red).

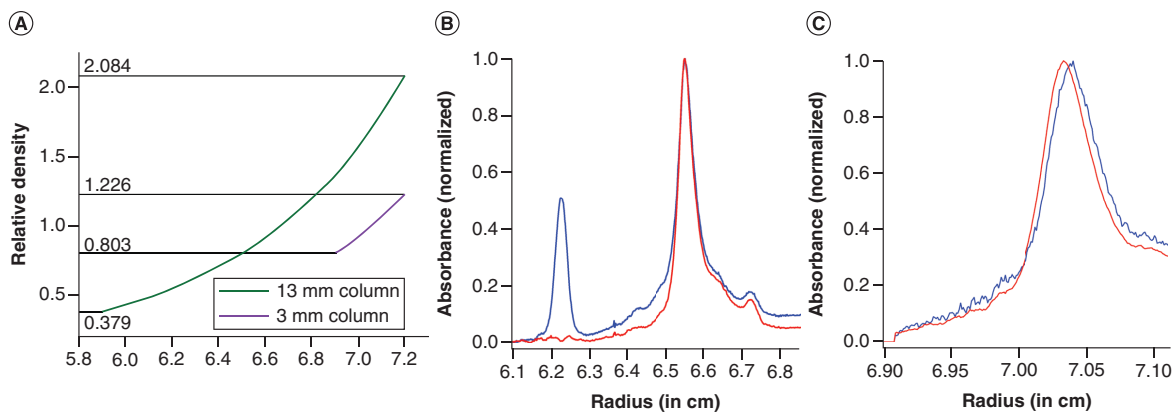


Figure 6. The effect of column length on CsCl gradient. (A) Simulated CsCl gradient formation in a 0.3-cm centerpiece filled with a 13-mm column (green) and 3-mm column (purple). CsCl gradients from long-column experiments (13 mm) provide a 3.6-fold higher dynamic density range than short-column experiments (3 mm). (B) 13-mm column experiment at 1.36 g/cm^3 CsCl, (C) 3-mm column experiment at 1.35 g/cm^3 CsCl. In (B) and (C) the DNA signal is shown in red and the protein signal in blue.

in the center of the solution column, providing baseline separation between the empty and full species, as well as the meniscus and bottom of the cell. At the highest CsCl concentration, the peak corresponding to empty capsids was no longer visible and floated to the top of the cell. At all three CsCl concentrations, the apparent density was approximately 1.20 g/cm^3 for empty AAVs and $1.30\text{--}1.43 \text{ g/cm}^3$ for the filled AAV capsid and higher-density peaks.

Rotor speed can also be used to modulate the CsCl gradient profile. In Figure 5A, an overlay of the CsCl equilibrium density gradient profile was simulated for three rotor speeds (40, 50, and 60 kr.p.m.), demonstrating the variation in the density profile. Sample AAV9:CAG-mNeonGreen 1 was measured at 50 and 60 kr.p.m. to demonstrate the resulting variations in peak positions (Figure 5B). At 50 kr.p.m., the gradient is shallower and tends to broaden the peaks, especially toward the bottom of the cell. At 50 kr.p.m., the gradient requires 9 h to reach equilibrium (4 h longer than at 60 kr.p.m.). The reduced speed slightly shifts the empty capsids to the left, while the filled AAV peaks are shifted to the right, closer to the bottom of the cell. Although a reduction in rotor speed reduces the density range over which AAV samples can be measured, this approach increases baseline separation and allows the investigator to focus on a particular density range with higher resolution.

The effect of CsCl column length was simulated with the ASTFEM simulation routine in UltraScan [45,46], calculating the CsCl distribution for a long (13-mm) column and a short (3-mm) column (Figure 6A). The variation in column length clearly demonstrates that at 60 kr.p.m., the CsCl gradient distribution in the long

column (13 mm) provides a 3.6-fold higher dynamic density range than the short column (3 mm). Although this approach was advocated by Sternisha *et al.* [33], we do not recommend to use short column centerpieces for ABDE experiments involving AAV, because the entire range of capsid-loading states cannot be distinguished by this approach. The ratio of the maximum density over the minimum density in a 13-mm column is 5.5, but only 1.5 for a 3-mm column. When measuring AAV9:CAG-mNeonGreen 1 in the 3-mm column, at 1.36 g/ml CsCl the sample did not sufficiently separate from the meniscus; therefore the CsCl density was reduced to 1.35 g/ml. At 1.35 g/ml, in contrast to the long-column experiments, only a single peak (likely corresponding to the filled capsid species) was observed in the short-column experiments (Figure 6B & C). Therefore the dynamic range of the 3-mm column experiments is insufficient to simultaneously detect empty, partially filled and filled AAV capsids in a single experiment. Overall, the best experimental design for AAV experiments employed a CsCl concentration of 1.36 g/ml at 60 kr.p.m., 20°C, using a long column (12–13 mm) in a 3-mm centerpiece, and measuring wavelengths 240–290 nm. It is recommended to use optically pure CsCl that does not absorb, such as UltraPure™ CsCl, optical grade (Thermo Fisher Scientific, cat. no. 15507023). In addition to background absorbance from CsCl, the high refractive index of CsCl can also contribute to background signal, which must be subtracted. To correctly account for the baseline contribution from any absorbance or refractive effects, it is advised to also measure the signal from a solution with an identical CsCl concentration in a separate channel. This reference channel absorbance can be used for all other channels in the same run that are performed at the same CsCl concentration. The baseline contribution from CsCl can then be removed from all samples in the experiment using the pseudo-absorbance program in UltraScan [30]. To further mitigate the effects of refractive artifacts from CsCl gradients, we recommend to shorten the optical path length by employing 3-mm centerpieces. In order to withstand high hydrostatic pressures at high speed and high CsCl densities, we recommend to use titanium centerpieces (Nanolytics Instruments), which are rated up to 60,000 r.p.m.

In our experiments, we have observed the presence of contaminants and refractive artifacts resulting from CsCl gradients that contribute to baseline variations, which are also dependent on wavelength (e.g., Figures 2, 4, 5, & 6). The intensity recordings from a single channel filled with CsCl at the same concentration and approximately the same loading volume as all other channels suffices to provide the necessary baseline correction data for the pseudo-absorbance conversion module in UltraScan [30]. In this context, it is important to understand that the radially invariant noise component of the last scan in an ABDE experiment, which is considered to be at equilibrium, is also time-invariant. Any systematic baseline contributions observed in the equilibrium scan can therefore be considered to be part of the time-invariant noise and handled with the algorithms discussed by Mortezaazadeh and Demeler [30].

Comparison of MW SV, ABDE & TEM

The ABDE, SV and TEM results were compared in order to demonstrate their equivalence. SV analysis of sample AAV8 BCM #1 revealed filled capsids sedimenting at 95 S (Figure 7A), along with a nucleic acid signal sedimenting below 20 S. The ABDE results (Figure 7B) show a major peak at 6.54 cm with a density of 1.29 g/cm³, corresponding to the filled capsids. Once again, two smaller higher-density peaks are found, at 6.66 and 6.74 cm, corresponding to densities of 1.34 and 1.38 g/cm³, respectively. When the deconvoluted protein and DNA signals are normalized to the amplitude of the filled capsid, it is clear that the two higher-density peaks share an identical protein:DNA ratio with the filled capsid peak. The identity of these higher-density peaks is not known. One possibility is that they represent overfilled capsids containing more than one complement of the DNA genome. This possibility was rejected because the MW analysis of both samples clearly demonstrated identical protein:DNA ratios in the higher-density peaks compared with the filled capsid peaks (Figure 7A). A larger capsid, accommodating more proteins and DNA, is also unlikely because the velocity data of AAV8 BCM #1 do not indicate the presence of any faster-sedimenting species. We speculate that the higher-density species are the result of a leaky capsid, allowing a small amount of CsCl to enter the capsid, binding to the DNA. The second species could be a capsid containing externalized DNA, or DNA or RNA fragments attached to the exterior of the capsids, freely complexed by CsCl, increasing the overall density of each species. For the TEM analysis, 1460 particles were counted (Figure 7C), and only two empty particles were identified.

SV analysis (Figure 7D) of AAV9:CAG-mNeonGreen 1 revealed a heterogeneous composition consisting of 55% filled capsids (95 S), 15% empty capsids (~60 S) and approximately 20% partially filled capsids (70–93 S) (Figure 7E). ABDE analysis of the same sample revealed a peak containing mostly protein signal, with a density of 1.20 g/cm³ at 6.25 cm (12.5% of the protein signal), corresponding to empty capsids. Between 6.35 and 6.54 cm, the protein and DNA absorbance gradually increases but never reaches a 1:1 ratio as observed in the filled capsids

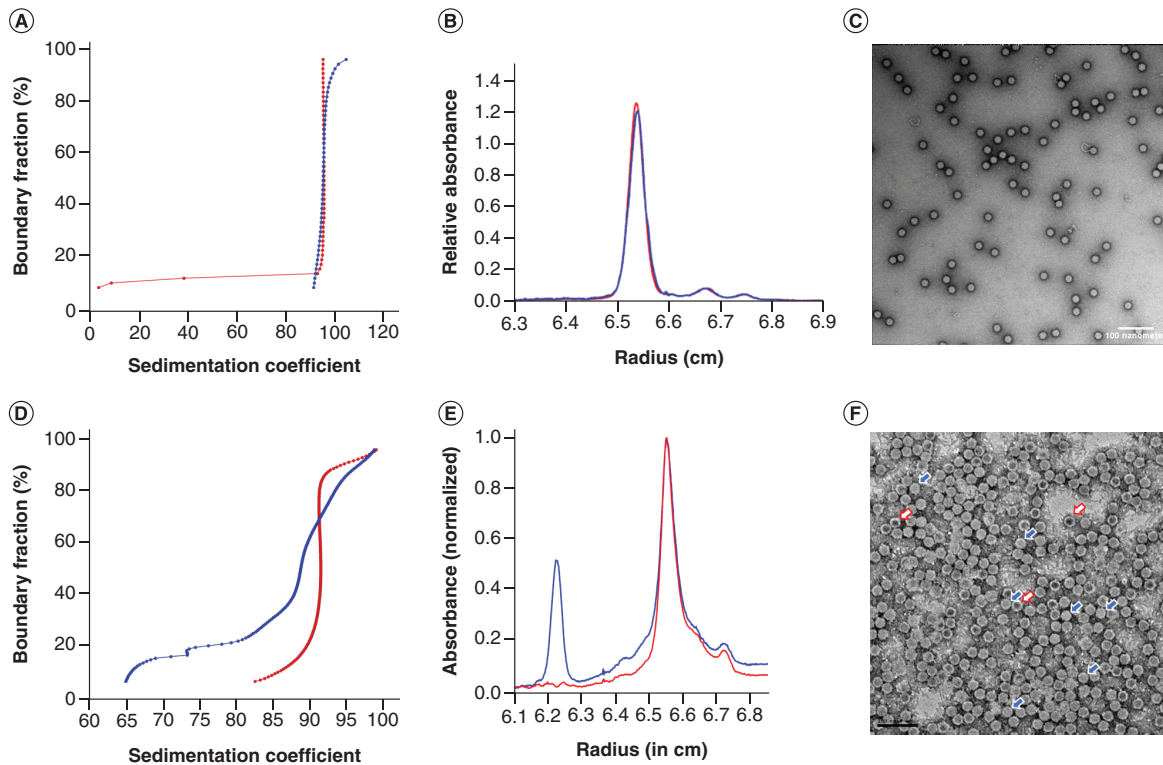


Figure 7. Adeno-associated virus formulations measured using sedimentation velocity and analytical buoyant density equilibrium multi-wavelength analytical ultracentrifugation, deconvoluted into its protein absorbance pattern (blue) and DNA absorbance pattern (red), and by transmission electron microscopy. The top panel shows AAV8 analyzed by (A) SV MW-AUC, (B) ABDE MW-AUC with protein and DNA deconvolutions normalized to 1.3 Optical density and (C) transmission electron microscopy; no empty AAVs are visible. The bottom panel shows AAV9:CAG mNeonGreen 2 analyzed by (D) SV MW-AUC, (E) ABDE MW-AUC with protein and DNA deconvolutions normalized to 1 OD and (F) transmission electron microscopy; the blue arrows show full AAVs and the red arrows empty AAVs.

AAV: Adeno-associated virus; ABDE: Analytical buoyant density equilibrium; MW-AUC: Multi-wavelength analytical ultracentrifugation; OD: Optical density; SV: Sedimentation velocity.

(6.57 cm). This suggests the presence of a heterogeneous mixture of partially filled capsids containing varying lengths of nucleic acids. The remaining three high density peaks, between 6.55 and 6.77 cm (corresponding to a density of 1.30–1.38 g/cm³, respectively) all exhibited a 1:1 ratio of protein:DNA. Together these peaks contribute approximately 51% of the protein signal, similar to the ratio of filled capsids identified by SV. By TEM, the sample was identified to contain approximately 20% empty capsids and around 80% filled capsids, but the method was unable to distinguish partially filled capsids (Figure 7F), likely counting partially filled capsids as filled capsids. Finally, an AAV5 preparation of empty capsid was compared by SV, ABDE and MP (Figure 8). The SV results showed a sedimentation coefficient of ~65 S, while the ABDE experiment resulted in a single peak at 6.19 cm and a density of 1.20 g/cm³. MP resulted in a single peak with a mass of 3797 kDa.

Discussion

Currently, the only well-established method with sufficient resolving power to detect empty, partially full and full AAV capsids in a single experiment is AUC [47,48]. However, single-wavelength AUC exhibits deficiencies in quantification and identification of sample species. In this study, we describe two improved AUC methods, SV and ABDE, leveraging MW detection, which can greatly improve accuracy, resolution and throughput and significantly reduce AAV sample requirements. Data acquisition and analysis with UltraScan automates the AUC data acquisition, analysis and reporting workflow and supports 21 CFR part 11 requirements to facilitate GMP integration. In addition, the high-performance computing possible with UltraScan greatly accelerates data processing. The results from these methods were compared with traditional 260/280 nm AUC experiments, cryo-TEM and MP

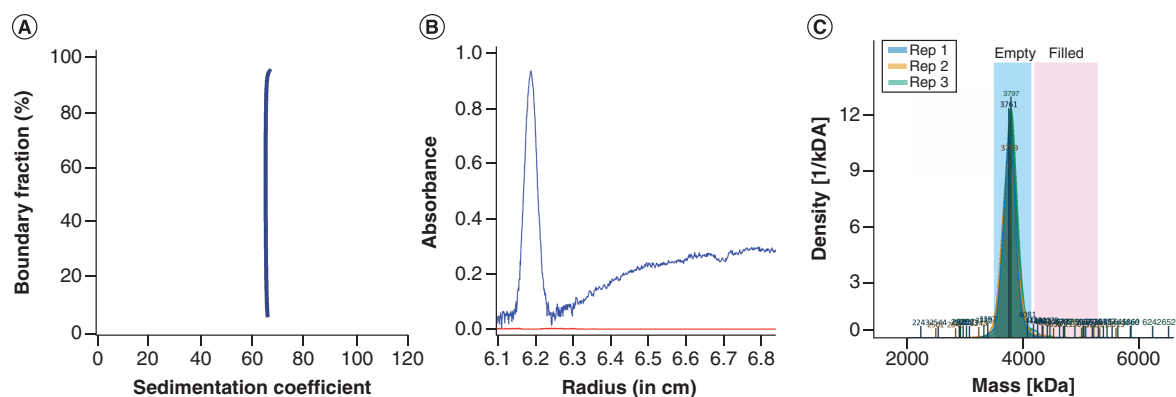


Figure 8. Comparison of AAV5 measured by sedimentation velocity and analytical buoyant density analytical ultracentrifugation and mass photometry. (A) Sedimentation velocity multi-wavelength analytical ultracentrifugation and (B) analytical buoyant density equilibrium multi-wavelength analytical ultracentrifugation. For both, after the spectral deconvolution only the protein signal (blue) was present. (C) Results from mass photometry measured in triplicate.

measurements, demonstrating significant improvements in accuracy and statistics. Finally, our study demonstrates that MW-AUC methods can be applied to multiple AAV serotypes and transgenes without modification, and potentially – with minor modifications to rotor speed, run length and CsCl concentration – to other viral vector systems. Our improvements addressed multiple limitations that prevent the widespread adoption of AUC methods for AAV characterization. The high AAV sample requirement for SV experiments is the most critical limitation. However, it should be noted that sample recovery after SV experiments is possible, to permit further testing. By switching to ABDE experiments, the required sample amount is significantly reduced by 20- to 40-fold. Two factors contribute to the significant sample reduction. The first factor relates to the differences by which the solutes are distributed throughout the cell in each experiment. In any AUC experiment, the measured signal should ideally match the dynamic range of the detector. The sample requirements to reach this limit are very different for the two experiments. In SV experiments, the loading concentration is uniformly distributed over the entire column length. In ABDE experiments, at equilibrium, the entire signal is concentrated into one or more narrow peaks. This concept is illustrated in [Supplementary Figure 4](#), where the orange shaded regions reflect the sample required to reach an OD of 0.4 in either experiment. Secondly, the lower sample requirements are a consequence of the enhanced signal-to-noise ratio achieved through the improved noise processing possible in UltraScan [30]. MW-AUC provides additional data points through observations at multiple wavelengths, increasing the accuracy and amplifying the signal-to-noise ratio through additional data points by combining all wavelengths in a global fit which separates the protein and DNA signals [20,21]. Because data are collected at equilibrium, a filled rotor with 16 samples can be measured at up to 100 wavelengths in the Optima AUC, greatly enhancing sensitivity and throughput at the same time.

MW-AUC offers an orthogonal verification through spectral deconvolution of protein and DNA signals to unambiguously identify and quantify AAV-loading states and other contaminants with the highest accuracy and reproducibility. This eliminates uncertainty about filled capsid ratios because the protein capsid can be identified without contribution from the DNA signal, providing an unambiguous mass ratio for each species. It also provides the spectral identity of contaminants, which is essential to assure drug purity and patient safety. The ability to simultaneously characterize the presence of contaminating species and quantify capsid ratios is an important benefit of the MW-AUC approach. SV experiments excel at simultaneously addressing a larger range of solute properties, useful for contaminant identification, but are limited by their throughput and higher sample requirements. For ABDE experiments, the relevant information is accessed after equilibrium has been reached, allowing not only more time for data collection at multiple wavelengths, but also for collection of additional cells and channels, significantly improving throughput. Our studies included a comparison with negative-stain TEM experiments, which showed excellent agreement when only full or empty capsids were present, but the presence of partially filled capsids could not be established by TEM.

ABDE experiments revealed a previously unknown feature of AAV capsids: the presence of two additional higher-density peaks with the same protein:DNA ratio as the full capsid (Figures 4A–C, 6B & 7B & E). We hypothesize that the higher-density peaks are a result of Cs ion complexation by DNA in potentially leaky capsids. Capsid instabilities under certain conditions have been reported earlier [49,50], pointing to a possible undesirable species in therapeutic formulations. Because CsCl and other density gradient-forming materials change the chemical environment of AAV capsids in terms of ionic strength compared with the physiological buffers used in SV experiments, and because these chemicals are commonly used to purify AAV capsids, further research is warranted to better understand the identity of these two higher-density species and the role of pH and CsCl in the solvent as factors potentially affecting capsid stability.

Conclusion

Our study demonstrates the relevance and reliability of SV and ABDE MW-AUC for the characterization and quantification of AAV-loading states in AAV serotypes 5, 8 and 9. It highlights the improved information obtained from MW analysis, demonstrating its abilities to detect correct ratios of empty, partially filled and full AAVs. The ABDE approach promises significant sample savings compared with the traditional SV method, and revealed additional species not seen in SV. The UltraScan software observes stringent requirements for 21 CFR Part 11 compliance in its design, facilitating current GMP integration and automation of sample analysis. Together, these advances will help reinforce AUC as the gold standard analysis method for viral vectors.

Summary points

- Multi-wavelength (MW) analytical ultracentrifugation (AUC) methods are presented for the quantification of adeno-associated virus capsid loading ratios and the identification of product-related impurities and contaminants.
- The presented methods correct errors encountered in dual-wavelength AUC, which over-emphasize filled capsids.
- In contrast to transmission electron microscopy, MW-AUC methods can detect and correctly quantify partially filled capsids.
- In contrast to mass photometry, MW analytical buoyant density equilibrium (ABDE) methods provide results that do not require reference standards; the densities of each peak are unique for each capsid loading state.
- MW-ABDE methods separate protein from DNA signal and allow proteinaceous capsids to be measured separately from the DNA.
- MW-ABDE methods require 20- to 40-fold less sample for comparable sensitivity as sedimentation velocity AUC.
- MW-ABDE methods offer significantly higher throughput by leveraging both channels in a centerpiece for sample measurement.
- MW-ABDE methods identified two new previously unknown high-density capsid species that may result from adeno-associated virus exposure to CsCl. Further research is needed to characterize these species.

Supplementary data

To view the supplementary data that accompany this paper please visit the journal website at: www.futuremedicine.com/doi/suppl/10.2217/nnm-2023-0156

Financial disclosure

This work received funding from the Beckman Institute CLOVER Center at Caltech and the NIH BRAIN Initiative Armamentarium (UF1MH128336), Canada 150 Research Chairs Program (C150-2017-00015), Canada Foundation of Innovation (CFI-37589), Canadian Natural Science and Engineering Research Council (DG-RGPIN-2019-05637), Cancer Prevention and Research Institute of Texas (RP190602), NIH-NIGMS (1R01GM120600), NSF (TG-MCB070039N) and the University of Texas (TG457201). The authors have no other relevant affiliations or financial involvement with any organization or entity with a financial interest in or financial conflict with the subject matter or materials discussed in the manuscript apart from those disclosed. This includes employment, consultancies, honoraria, stock ownership or options, expert testimony, grants or patents received or pending, or royalties.

Competing interests disclosure

The authors have no competing interests or relevant affiliations with any organization or entity with the subject matter or materials discussed in the manuscript. This includes employment, consultancies, honoraria, stock ownership or options, expert testimony, grants or patents received or pending, or royalties.

Writing disclosure

No writing assistance was utilized in the production of this manuscript.

Data availability statement

The UltraScan software used to analyze the AUC data is open source and freely available from the Github repository (<https://github.com/ehb54/ultrascan3>). The AUC data are available in openAUC format upon request from the authors and are stored in the UltraScan LIMS server at the Canadian Center for Hydrodynamics.

References

Papers of special note have been highlighted as: ● of interest; ●● of considerable interest

1. Ma CC, Wang ZL, Xu T, He ZY, Wei YQ. The approved gene therapy drugs worldwide: from 1998 to 2019. *Biotechnol. Adv.* 40, 107502 (2020).
2. US Food and Drug Administration. Approved cellular and gene therapy products. www.fda.gov/vaccines-blood-biologics/cellular-gene-therapy-products/approved-cellular-and-gene-therapy-products
3. ClinicalTrials.gov. Gene therapy clinical trials. <https://clinicaltrials.gov/ct2/results?cond=&term=gene+therapy&cntry=&state=&city=&dist=>
4. Wang D, Tai PW, Gao G. Adeno-associated virus vector as a platform for gene therapy delivery. *Nat. Rev. Drug Discov.* 18, 358–378 (2019).
5. Li C, Samulski RJ. Engineering adeno-associated virus vectors for gene therapy. *Nat. Rev. Genet.* 21, 255–272 (2020).
6. Wörner TP, Bennet A, Habka S *et al.* Adeno-associated virus capsid assembly is divergent and stochastic. *Nat. Commun.* 12, 1642 (2021).
7. Pei X, Earley LF, He Y *et al.* Efficient capsid antigen presentation from adeno-associated virus empty virions *in vivo*. *Front. Immunol.* 9, 844 (2018).
8. Wright JF. Product-related impurities in clinical-grade recombinant AAV vectors: characterization and risk assessment. *Biomedicines* 2, 80–97 (2014).
9. Colomb-Delsuc M, Raim R, Fiedler C *et al.* Assessment of the percentage of full recombinant adeno-associated virus particles in a gene therapy drug using CryoTEM. *PLOS ONE* 17(6), e0269139 (2022).
10. Wu D, Hwang P, Li T, Piszczek G. Rapid characterization of adeno-associated virus (AAV) gene therapy vectors by mass photometry. *Gene Ther.* 29(12), 691–697 (2022).
11. Gimpel AL, Katsikis G, Sha S *et al.* Analytical methods for process and product characterization of recombinant adeno-associated virus-based gene therapies. *Mol. Ther. Methods Clin. Dev.* 20, 740–754 (2021).
12. Mayginnes JP, Reed SE, Berg HG *et al.* Quantitation of encapsidated recombinant adeno-associated virus DNA in crude cell lysates and tissue culture medium by quantitative, real-time PCR. *J. Virol. Methods* 137, 193–204 (2006).
13. Fagone P, Wright JF, Nathwani AC *et al.* Systemic errors in quantitative polymerase chain reaction titration of self-complementary adeno-associated viral vectors and improved alternative methods. *Hum. Gene Ther. Methods* 23, 1–7 (2012).
14. Yarawsky AE, Zai-Rose V, Cunningham HM *et al.* AAV analysis by sedimentation velocity analytical ultracentrifugation: beyond empty and full capsids. *Eur. Biophys. J.* 52(4–5), 353–366 (2023).
15. Hayes DB, Dobnik D. Commentary: multiplex dPCR and SV-AUC are promising assays to robustly monitor the critical quality attribute of AAV drug product integrity. *J. Pharm. Sci.* 111(8), 2143–2148 (2022).
16. Savelyev A, Gorbet GE, Henrickson A, Demeler B. Moving analytical ultracentrifugation software to a good manufacturing practices (GMP) environment. *PLOS Comput. Biol.* 16, e1007942 (2020).
17. Werle AK, Powers TW, Zobel JF *et al.* Comparison of analytical techniques to quantitate the capsid content of adeno-associated viral vectors. *Mol. Ther. Methods Clin. Dev.* 23, 254–262 (2021).
18. Richter K, Wurm C, Strasser K *et al.* Purity and DNA content of AAV capsids assessed by analytical ultracentrifugation and orthogonal biophysical techniques. *Eur. J. Pharm. Biopharm.* 189, 68–83 (2023).
19. Berkowitz SA, Philo JS. Monitoring the homogeneity of adenovirus preparations (a gene therapy delivery system) using analytical ultracentrifugation. *Anal. Biochem.* 362, 16–37 (2007).
20. Gorbet GE, Pearson JZ, Demeler AK, Cölfen H, Demeler B. Next-generation AUC: analysis of multiwavelength analytical ultracentrifugation data. *Methods Enzymol.* 562, 27–47 (2015).
21. Henrickson A, Gorbet GE, Savelyev A *et al.* Multi-wavelength analytical ultracentrifugation of biopolymer mixtures and interactions. *Anal. Biochem.* 652, 114728 (2022).
- **The multiwavelength analytical ultracentrifugation (AUC) technology is explained here and provides a fundamental basis for the understanding of the current manuscript.**
22. Khasa H, Kilby G, Chen X, Wang C. Analytical band centrifugation for the separation and quantification of empty and full AAV particles. *Mol. Ther. Methods Clin. Dev.* 21, 585–591 (2021).

23. Maruno T, Ishii K, Torisu T, Uchiyama S. Size distribution analysis of the adeno-associated virus vector by the c(s) analysis of band sedimentation analytical ultracentrifugation with multiwavelength detection. *J. Pharm. Sci.* 112, 937–946 (2023).
24. Maruno T, Usami K, Ishii K, Torisu T, Uchiyama S. Comprehensive size distribution and composition analysis of adeno-associated virus vector by multiwavelength sedimentation velocity analytical ultracentrifugation. *J. Pharm. Sci.* 110, 3375–3384 (2021).
25. Horne CR, Henrickson A, Demeler B, Dobson RC. Multi-wavelength analytical ultracentrifugation as a tool to characterise protein–DNA interactions in solution. *Eur. Biophys. J.* 49, 819–827 (2020).
26. Horne CR, Venugopal H, Panjekar S *et al.* Mechanism of NanR gene repression and allosteric induction of bacterial sialic acid metabolism. *Nat. Commun.* 12, 1988 (2021).
27. Gabir H, Gupta M, Meier M *et al.* Investigation of dynamic solution interactions between NET-1 and UNC-5B by multi-wavelength analytical ultracentrifugation. *Eur. Biophys. J.* 52(4–5), 473–481 (2023).
28. Ahmed I, Hahn J, Henrickson A *et al.* Structure–function studies reveal ComEA contains an oligomerization domain essential for transformation in Gram-positive bacteria. *Nat. Commun.* 13, 7724 (2022).
29. Demeler B, Gorbet GE. Chapter 8: analytical ultracentrifugation data analysis with UltraScan-III. In: *Analytical Ultracentrifugation: Instrumentation, Software, and Applications*. Uchiyama S, Arisaka F, Stafford W, Laue T (Eds). Springer, Tokyo, 119–143 (2016).
- **The UltraScan software package is a comprehensive hydrodynamic characterization toolkit that is open source and freely available, and used for all analysis performed in this manuscript.**
30. Mortezaadeh S, Demeler B. Systematic noise removal from analytical ultracentrifugation data with UltraScan. *Eur. Biophys. J.* 52(4–5), 203–213 (2023).
- **The pseudo-absorbance conversion module allows intensity to be used for equilibrium experiments and essentially doubles the capacity of the AUC analytical buoyant density equilibrium technique by removing time-invariant and baseline noise contributions.**
31. Savelyev A, Brookes EH, Henrickson A, Demeler B. A new UltraScan module for the characterization and quantification of analytical buoyant density equilibrium experiments to determine AAV capsid loading. *Eur. Biophys. J.* 52(4–5), 311–320 (2023).
- **The analytical buoyant density equilibrium peak integration tool described here is a logical module to be used for the rigorous quantification of adeno-associated virus capsid-loading states.**
32. Mortezaadeh S, Demeler B. A spectral decomposition quality assessment tool for multi-wavelength AUC experiments with UltraScan. *Eur. Biophys. J.* 52(4–5), 303–310 (2023).
- **The spectral decomposition viewer is used to monitor the multi-wavelength decomposition of AUC data to ensure an adequate fit quality.**
33. Sternisha SM, Wilson AD, Bouda E, Bhattacharya A, VerHeul R. Optimizing high-throughput viral vector characterization with density gradient equilibrium analytical ultracentrifugation. *Eur. Biophys. J.* 52(4–5), 387–392 (2023).
34. Bepperling A, Best J. Comparison of three AUC techniques for the determination of the loading status and capsid titer of AAVs. *Eur. Biophys. J.* 52(4–5), 401–413 (2023). Epub 2023 May 28.
- **The authors reach similar conclusions for various AUC techniques applied to adeno-associated virus characterization.**
35. Deng S, Oka K. Adeno-associated virus as gene delivery vehicle into the retina. *Methods Mol. Biol.* 2092, 77–90 (2020).
36. Ayuso E, Mingozzi F, Montane J *et al.* High AAV vector purity results in serotype- and tissue-independent enhancement of transduction efficiency. *Gene Ther.* 17, 503–510 (2010).
37. Challis RC, Kumar SR, Chan KY *et al.* Systemic AAV vectors for widespread and targeted gene delivery in rodents. *Nat. Protoc.* 14, 379–414 (2019).
38. Kumar SR, Miles TF, Chen X *et al.* Multiplexed Cre-dependent selection yields systemic AAVs for targeting distinct brain cell types. *Nat. Methods* 17(5), 541–550 (2020).
39. Berkowitz SA, Laue T. Boundary convection during sedimentation velocity in the Optima analytical ultracentrifuge. *Anal. Biochem.* 631, 114306 (2021).
40. Demeler B. Methods for the design and analysis of sedimentation velocity and sedimentation equilibrium experiments with proteins. *Curr. Protoc. Protein Sci.* 60, 7.13.1–7.13.24 (2010).
41. Brookes EH, Boppana RV, Demeler B. Computing large sparse multivariate optimization problems with an application in biophysics. In: *SC'06: Proceedings of the 2006 ACM/IEEE Conference on Supercomputing*. IEEE, Tampa, FL, USA (2006).42–42
42. Brookes E, Cao W, Demeler B. A two-dimensional spectrum analysis for sedimentation velocity experiments of mixtures with heterogeneity in molecular weight and shape. *Eur. Biophys. J.* 39, 404–414 (2010).
43. Demeler B, van Holde KE. Sedimentation velocity analysis of highly heterogeneous systems. *Anal. Biochem.* 335, 279–288 (2004).
44. Schuck P, Demeler B. Direct sedimentation analysis of interference optical data in analytical ultracentrifugation. *Biophys. J.* 76, 2288–2296 (1999).
45. Cao W, Demeler B. Modeling analytical ultracentrifugation experiments with an adaptive space–time finite element solution of the Lamm equation. *Biophys. J.* 89, 1589–1602 (2005).

46. Cao W, Demeler B. Modeling analytical ultracentrifugation experiments with an adaptive space–time finite element solution for multicomponent reacting systems. *Biophys. J.* 95, 54–65 (2008).
47. Burnham B, Nass S, Kong E *et al.* Analytical ultracentrifugation as an approach to characterize recombinant adeno-associated viral vectors. *Hum. Gene Ther. Methods* 26, 228–242 (2015).
48. Fu X, Chen WC, Argento C *et al.* Analytical strategies for quantification of adeno-associated virus empty capsids to support process development. *Hum. Gene Ther. Methods* 30, 144–152 (2019).
49. Bernaud J, Rossi A, Fis A *et al.* Characterization of AAV vector particle stability at the single-capsid level. *J. Biol. Phys.* 44, 181–194 (2018).
50. Ros C, Baltzer C, Mani B, Kempf C. Parvovirus uncoating *in vitro* reveals a mechanism of DNA release without capsid disassembly and striking differences in encapsidated DNA stability. *Virology* 345, 137–147 (2006).